THE ASTROPHYSICAL JOURNAL, 204:573–581, 1976 March 1


# SOLAR MAGNETO-ATMOSPHERIC WAVES. I. AN EXACT SOLUTION FOR A HORIZONTAL MAGNETIC FIELD

ALAN H. NYE AND JOHN H. THOMAS*
Department of Mechanical and Aerospace Sciences, University of Rochester
*Received 1975 June 20; revised 1975 August 7*

## ABSTRACT

The linearized theory of magneto-atmospheric waves (involving the combined restoring forces due to buoyancy, compressibility, and magnetic field) is developed for the case of a horizontal magnetic field. A general propagation equation is derived for adiabatic perturbations with arbitrary vertical distributions of the sound speed $c$, Alfvén velocity $v_A$, and local density scale height $H$. An exact analytical solution to the propagation equation is obtained for the case of an isothermal atmosphere permeated by a uniform horizontal magnetic field, without making the usual short-wavelength assumption. This solution is applied to an idealized model of the low-corona–chromosphere transition region for comparison with observations of flare-induced coronal waves. The results show that disturbances may propagate horizontally in the low corona in a wave guide formed by the sudden density increase into the chromosphere below and by the rapidly increasing Alfvén velocity with height in the corona. The group velocity of the guided wave modes is nearly independent of wavelength, so that a disturbance propagates as a compact wave packet.

*Subject headings:* hydromagnetics — Sun: atmospheric motions — Sun: corona — Sun: magnetic fields

## I. INTRODUCTION

The theory of waves in a compressible, stratified, electrically conducting atmosphere permeated by a magnetic field is of considerable importance in astrophysics, especially in solar physics where there is a wealth of detailed observations of such waves in the solar atmosphere. Following Yu (1965), we shall refer to waves which involve compressibility, buoyancy, and magnetic forces as *magneto-atmospheric waves*. Among the many solar phenomena that are seemingly attributable to magneto-atmospheric waves are the heating of the corona and of chromospheric plages, the 5-minute oscillations in active regions, oscillations in sunspot umbrae and penumbrae, and flare-induced coronal disturbances.

The theory of magneto-atmospheric waves is complicated by the anisotropic nature of the medium; the gravitational field and the magnetic field each introduce preferred directions. Additionally, the disturbance is subjected to the combined restoring forces due to compressibility, buoyancy, and the magnetic field, so that pure wave modes (i.e., acoustic, Alfvén, and gravity) exist only as special cases. In general, magneto-atmospheric waves involve the effects of all three restoring forces. The problem is compounded by the fact that the basic parameters describing wave propagation in the solar atmosphere (the sound speed $c$, the Alfvén velocity $v_A$, and the local density scale height $H$) are, in general, functions of height, and therefore the disturbance cannot be represented by plane waves propagating in the atmosphere.

Previously, the problem of magneto-atmospheric waves has been studied by either of two basic approaches, each yielding a dispersion relation based on constant values of the atmospheric parameters. The first approach has been to assume that the vertical extent of the disturbance is much less than the smallest scale height for variation of the atmospheric parameters. The parameters can then be taken as constant locally. McLellan and Winterberg (1968) studied an isothermal atmosphere permeated by a uniform magnetic field with arbitrary orientation. Then, assuming that the Alfvén velocity is constant locally (although it actually increases exponentially with height), they derived a local dispersion relation that is valid for short wavelengths (short compared with the density scale height). This local dispersion relation has been studied by several authors (Bel and Mein 1971; Michalitsanos 1973; Nakagawa *et al.* 1973) to determine the effects of different propagation directions and magnetic field orientations.

The second basic approach has been to investigate an isothermal atmosphere permeated by a horizontal magnetic field that decreases exponentially with height such that the Alfvén velocity is constant, as are the sound speed and the density scale height. Yu (1965) derived the dispersion relation which in this case is valid for all wavelengths. He evaluated the three modes of propagation for various angles between the wave propagation vector and the magnetic field. Chen and Lykoudis (1972) used the dispersion relation of Yu to study the 5-minute oscillations in plage regions. Nye and Thomas (1974*a*) used Yu's dispersion relation in connection with a multilayer model for running penumbral waves.

* Also C. E. Kenneth Mees Observatory.

We consider only plane-parallel atmospheres, with no horizontal variation, in order to permit Fourier decomposition in the horizontal directions as well as time. With variations in the $z$-direction only, the governing partial differential equations reduce to ordinary differential equations. There are only two magnetic field configurations consistent with static equilibrium and no horizontal variation. They are $\boldsymbol{B}$ = constant and $\boldsymbol{B} = [B_x(z), B_y(z), 0]$. We shall restrict our study to the case of a unidirectional horizontal magnetic field that may vary with height. We shall not follow either of the two basic approaches discussed above, however, because of the inherent limitations of each of them for solar applications. The length scale for magnetic field changes in the solar atmosphere is generally much greater than the density scale height, so that the assumption of constant Alfvén velocity is not justified. On the other hand, the length scale of observed disturbances in the solar atmosphere is not generally small compared with the density scale height. This is especially true in the photosphere where the density scale height may be smaller than 100 km, and hence smaller than the limit of observational resolution.

In § II we derive a general propagation equation for an arbitrary direction of propagation and arbitrary vertical variations of the atmospheric parameters. For the case of an isothermal atmosphere permeated by a uniform horizontal magnetic field, the Alfvén velocity increases exponentially with height. In § III we obtain an exact general solution of the propagation equation in this case. We compute eigenmodes for the case of a rigid lower boundary in § IV, and apply this to a specific solar wave phenomenon, the flare-induced coronal waves, in § V.

The analytical treatment in §§ II and III also forms the basis of a following paper in which we deal with running penumbral waves.

## II. BASIC EQUATIONS

The atmosphere is assumed to be a compressible, inviscid, perfectly conducting gas under a uniform acceleration of gravity $\boldsymbol{g}$ ($=0.274$ km s$^{-2}$) in the negative $z$-direction. The undisturbed magnetic field is taken in the $x$-direction and may vary with height $z$; i.e., $\boldsymbol{B}_0 = [B_0(z), 0, 0]$. The undisturbed pressure, density, and temperature may all be functions of height $z$, and are denoted by $p_0(z)$, $\rho_0(z)$, and $T_0(z)$, respectively. We shall see that wave propagation in the basic atmosphere may be completely characterized by the vertical variation of the sound speed $c(z)$, the Alfvén velocity $v_A(z)$, and the local density scale height $H(z)$, defined by

$$c^2 \equiv \left(\frac{\partial p_0}{\partial \rho_0}\right)_s, \qquad v_A{}^2 \equiv \frac{B_0{}^2}{4\pi\rho_0}, \qquad \frac{1}{H} \equiv -\frac{1}{\rho_0}\frac{d\rho_0}{dz}. \tag{1}$$

The unperturbed atmosphere is taken to be in static equilibrium:

$$\frac{d}{dz}\left(p_0 + \frac{B_0{}^2}{8\pi}\right) = -\rho_0 g. \tag{2}$$

If the magnetic field is a function of height $z$, then it has a role in the basic equilibrium of the atmosphere. We consider only stable atmospheres, which requires that

$$\frac{dT_0}{dz} - \left(\frac{dT_0}{dz}\right)_s > -\frac{1}{\rho_0 R}\frac{d}{dz}\left(\frac{B_0{}^2}{8\pi}\right),$$

where $(dT_0/dz)_s$ is the adiabatic temperature gradient and $R$ is the gas constant (see Thomas and Nye 1975 for a recent discussion).

Consider small adiabatic perturbations of the equilibrium atmosphere, letting $p$, $\rho$, $\boldsymbol{u}$, and $\boldsymbol{B}$ denote the perturbations in pressure, density, velocity, and magnetic field, respectively. Then, the basic linearized equations of continuity, momentum, energy, and induction are

$$\frac{\partial \rho}{\partial t} + \nabla\cdot(\rho_0 \boldsymbol{u}) = 0, \tag{3}$$

$$\rho_0 \frac{\partial \boldsymbol{u}}{\partial t} + \nabla p - \rho \boldsymbol{g} - \frac{1}{4\pi}[(\nabla \times \boldsymbol{B}_0) \times \boldsymbol{B} + (\nabla \times \boldsymbol{B}) \times \boldsymbol{B}_0] = 0, \tag{4}$$

$$\frac{\partial p}{\partial t} + \boldsymbol{u}\cdot\nabla p_0 = c^2\left(\frac{\partial \rho}{\partial t} + \boldsymbol{u}\cdot\nabla\rho_0\right), \tag{5}$$

$$\frac{\partial \boldsymbol{B}}{\partial t} - \nabla \times (\boldsymbol{u} \times \boldsymbol{B}_0) = 0. \tag{6}$$

After taking the time derivative of the momentum equation (4), we may eliminate the perturbation quantities $p$, $\rho$, and $\boldsymbol{B}$ by using equations (3), (5), and (6). This leaves a single vector equation for the velocity perturbation $\boldsymbol{u} = (u, v, w)$:

$$\rho_0 \frac{\partial^2 \boldsymbol{u}}{\partial t^2} + \nabla\left[\rho_0 w\left(g + \frac{1}{8\pi\rho_0}\frac{dB_0^2}{dz}\right) - c^2\rho_0\nabla\cdot\boldsymbol{u}\right] + [(\boldsymbol{u}\cdot\nabla)\rho_0 + \rho_0\nabla\cdot\boldsymbol{u}]\boldsymbol{g}$$
$$- \frac{1}{4\pi}[[(\nabla\times\boldsymbol{B}_0)\times[\nabla\times(\boldsymbol{u}\times\boldsymbol{B}_0)] - \boldsymbol{B}_0\times\{\nabla\times[\nabla\times(\boldsymbol{u}\times\boldsymbol{B}_0)]\}]] = 0\,. \quad (7)$$

Next, we assume that the perturbation velocity has the form $\boldsymbol{u} = \hat{\boldsymbol{u}}\exp i(\boldsymbol{k}\cdot\boldsymbol{r} - \omega t)$, with $\hat{\boldsymbol{u}} = \hat{\boldsymbol{u}}(z) = [\hat{u}(z), \hat{v}(z), \hat{w}(z)]$ and $\boldsymbol{k}\cdot\boldsymbol{r} = k_x x + k_y y$. Then, using the definition of $v_A^2$, the three components of the momentum equation (7) become

$$(\omega^2 - c^2k_x^2)\hat{u} - c^2k_xk_y\hat{v} - ik_x\left(g - c^2\frac{d}{dz}\right)\hat{w} = 0\,, \quad (8)$$

$$-c^2k_xk_y\hat{u} + [\omega^2 - c^2k_y^2 - v_A^2(k_x^2 + k_y^2)]\hat{v} - ik_y\left[g - (c^2 + v_A^2)\frac{d}{dz}\right]\hat{w} = 0\,, \quad (9)$$

and

$$ik_x\left(\frac{dc^2}{dz} - \frac{c^2}{H} + g + c^2\frac{d}{dz}\right)\hat{u} + ik_y\left[\frac{d}{dz}(c^2 + v_A^2) - \frac{(c^2 + v_A^2)}{H} + g + (c^2 + v_A^2)\frac{d}{dz}\right]\hat{v}$$
$$+ (c^2 + v_A^2)\frac{d^2\hat{w}}{dz^2} + \left[\frac{d}{dz}(c^2 + v_A^2) - \frac{(c^2 + v_A^2)}{H}\right]\frac{d\hat{w}}{dz} + (\omega^2 - v_A^2k_x^2)\hat{w} = 0\,. \quad (10)$$

These are the linearized perturbation equations. They give important information about particle motions for various modes of propagation in the atmosphere.

The horizontal components of the perturbation velocity can be eliminated from the system of equations (8)–(10) to yield a single equation for the vertical velocity $\hat{w}$. The resulting equation is

$$\frac{d^2\hat{w}}{dz^2} + A(z)\frac{d\hat{w}}{dz} + B(z)\hat{w} = 0\,, \quad (11)$$

where the coefficient $A(z)$ and $B(z)$ are given by

$$A(z) = -\frac{1}{H} + \frac{\omega^4}{DE}(\omega^2 - v_A^2k_x^2)^2\frac{dc^2}{dz} + \frac{1}{D}\left[-\omega^4 + (\omega^2 - c^2k_x^2)(\omega^2 - v_A^2k_x^2)\left(1 + \frac{\omega^4}{E}\right)\right]\frac{dv_A^2}{dz} \quad (12)$$

and

$$B(z) = \frac{1}{D}\left\{\omega^6 - [(c^2 + v_A^2)(k_x^2 + k_y^2) + v_A^2k_x^2]\omega^4\right.$$
$$+ \left[v_A^2k_x^2(k_x^2 + k_y^2)(2c^2 + v_A^2) - g(k_x^2 + k_y^2)\left(g - \frac{c^2}{H}\right) + \frac{g}{H}v_A^2k_y^2\right]\omega^2$$
$$\left. - v_A^2k_x^2(k_x^2 + k_y^2)\left[c^2v_A^2k_x^2 - g\left(g - \frac{c^2}{H}\right)\right] - \frac{g}{E}(\omega^2 - v_A^2k_x^2)^2\omega^2(k_x^2 + k_y^2)\frac{dc^2}{dz} - \frac{\omega^6}{E}k_y^2g\frac{dv_A^2}{dz}\right\}. \quad (13)$$

Here, $D$ and $E$ are given by

$$D = (\omega^2 - v_A^2k_x^2)[\omega^2(c^2 + v_A^2) - c^2v_A^2k_x^2] \quad (14)$$

and

$$E = \omega^4 - (k_x^2 + k_y^2)[\omega^2(c^2 + v_A^2) - c^2v_A^2k_x^2]\,. \quad (15)$$

Equation (11) is a general equation for the vertical component of velocity for a perturbation propagating in an arbitrary direction, in an atmosphere with a horizontal magnetic field and arbitrary vertical distributions of $c^2$, $v_A^2$, and $H$. This propagation equation has been given previously (Nye and Thomas 1974*a*) in the case $k_y = 0$.

### III. ISOTHERMAL ATMOSPHERE WITH A UNIFORM HORIZONTAL MAGNETIC FIELD

Now consider the case where the undisturbed temperature and magnetic field are constant with height. Since the magnetic field is uniform, it has no effect on the hydrostatic equilibrium of the atmosphere, and the equilibrium pressure and density both decrease exponentially with height. The sound speed and the density scale height are both constant, with values determined by the temperature of the atmosphere. The Alfvén velocity increases exponentially with height due to the decreasing density. The sound speed, density scale height, density, and Alfvén velocity are given by

$$c = (\gamma RT_0)^{1/2} = \text{const.}, \tag{16}$$

$$H = \frac{RT_0}{g} = \text{const.}, \tag{17}$$

$$\rho_0(z) = \rho_{00} e^{-z/H}, \tag{18}$$

and

$$v_A(z) = v_0 e^{z/2H}, \tag{19}$$

where $\rho_{00}$ and $v_0$ are the values of the undisturbed density and Alfvén velocity at $z = 0$.

The nondimensional parameter $\beta^2 \equiv v_0^2/c^2$ is introduced as a measure of the relative importance of the restoring forces due to the magnetic field and to compressibility at the point $z = 0$. For values of $\beta^2 < 1$, there is a region of the atmosphere above $z = 0$ where compressibility has more importance as a restoring force than does the magnetic force, but in any case the magnetic field always becomes dominant as $z$ becomes large.

In the remainder of this paper we shall consider only waves whose horizontal component of propagation is parallel to the magnetic field ($k_y = 0$). Using (16)–(19), we may write (11) as

$$[c^2\omega^2 + (\omega^2 - c^2k_x^2)v_0^2e^{z/H}]\frac{d^2\hat{w}}{dz^2} - \frac{c^2\omega^2}{H}\frac{d\hat{w}}{dz} + \left[(\omega^2 - c^2k_x^2)(\omega^2 - v_0^2e^{z/H}k_x^2) - g\left(g - \frac{c^2}{H}\right)k_x^2\right]\hat{w} = 0. \tag{20}$$

We define the nondimensional frequency $\Omega$ and the nondimensional horizontal wavenumber $K$ by

$$\Omega \equiv H\omega/c, \qquad K \equiv Hk_x. \tag{21}$$

By transforming the dependent and independent variables according to

$$W = \hat{w}e^{zK/H}, \qquad x = \frac{\Omega^2}{\beta^2(K^2 - \Omega^2)}e^{-z/H}, \tag{22}$$

we may put equation (20) in the dimensionless form

$$x(1 - x)\frac{d^2W}{dx^2} + [C - (A + B + 1)x]\frac{dW}{dx} - ABW = 0, \tag{23}$$

with

$$A + B = C = 2K + 1, \qquad AB = \Omega^2 + K + \left(\frac{\gamma - 1}{\gamma^2}\right)\frac{K^2}{\Omega^2}. \tag{24}$$

Equation (23) is the standard form of the hypergeometric differential equation.[1] The solutions of this equation may be expressed in terms of hypergeometric functions, given for $|x| < 1$ by

$$F(A, B; C; x) = \frac{\Gamma(C)}{\Gamma(A)\Gamma(B)}\sum_{n=0}^{\infty}\frac{\Gamma(A + n)\Gamma(B + n)}{\Gamma(C + n)}\frac{x^n}{n!}. \tag{25}$$

The general solution of equation (23) may be written, for $|x| < 1$, in terms of the original variables $z$ and $\hat{w}(z)$ as

$$\hat{w}(z) = D_1e^{-zK/H}F\left[A, B; C; \frac{\Omega^2}{\beta^2(K^2 - \Omega^2)}e^{-z/H}\right] + D_2e^{zK/H}\left[\frac{\beta^2(K^2 - \Omega^2)}{\Omega^2}\right]^{2K}F\left[A - C + 1, B - C + 1; 2 - C; \frac{\Omega^2}{\beta^2(K^2 - \Omega^2)}e^{-z/H}\right], \tag{26}$$

where $D_1$ and $D_2$ are arbitrary constants.

[1] The hypergeometric nature of the wave equation in this case was noted by us earlier (Nye and Thomas 1974*b*), and also independently by Adam (1975).

## IV. EIGENMODES FOR A RIGID LOWER BOUNDARY

We now examine modes of propagation in the relatively simple case of an isothermal atmosphere with a uniform horizontal magnetic field, bounded from below by a rigid wall at $z = 0$. The general solution (26) is subject to boundary conditions at $z = 0$ [$x = \Omega^2/\beta^2(K^2 - \Omega^2)$] and at $z = \infty$ ($x = 0$).

As a condition at $z = \infty$, we require that the total energy of the perturbation be integrable over $0 \leq z < \infty$. The magnetic energy of the perturbation is proportional to the square of the velocity. Since

$$\lim_{x \to 0} F(\alpha, \beta; \gamma; x) = 1 , \tag{27}$$

we see from equation (26) that we must take $D_2 = 0$.

The second boundary condition is that the vertical velocity vanish at the rigid wall, i.e., $\hat{w} = 0$ at $z = 0$, i.e., at $x = \Omega^2/\beta^2(K^2 - \Omega^2)$. Provided

$$\left| \frac{\Omega^2}{\beta^2(K^2 - \Omega^2)} \right| < 1 , \tag{28}$$

we may apply this condition directly to equation (26) with $D_2 = 0$ to obtain the dispersion relation

$$F\left[A, B; C; \frac{\Omega^2}{\beta^2(K^2 - \Omega^2)}\right] = 0 . \tag{29}$$

If, however, (28) is not satisfied, then other representations of the general solution (26), valid for $|x| \geq 1$, must be used in order to apply the boundary condition at $z = 0$. For

$$\frac{\Omega^2}{\beta^2(K^2 - \Omega^2)} \geq 1 , \tag{30}$$

the interval $0 \leq x \leq \Omega^2/\beta^2(K^2 - \Omega^2)$ contains the regular singular point at $x = 1$, and no solution that satisfies the boundary conditions and is also regular at $x = 1$ is to be expected. For the range

$$\frac{\Omega^2}{\beta^2(K^2 - \Omega^2)} \leq -1 , \tag{31}$$

we may use analytic continuation to extend the general solution (26). The analytic continuation of (26) with $D_2 = 0$, valid for $x \leq -1$, is given by

$$\hat{w}(z) = D_1 e^{-zK/H} \left\{ \frac{\Gamma(C)\Gamma(B - A)}{[\Gamma(B)]^2} \left[\frac{\beta^2(\Omega^2 - K^2)}{\Omega^2}\right]^A e^{zA/H} F\left[A, 1 - B; 1 - B + A; \frac{\beta^2(K^2 - \Omega^2)}{\Omega^2} e^{z/H}\right] \right.$$
$$\left. + \frac{\Gamma(C)\Gamma(A - B)}{[\Gamma(A)]^2} \left[\frac{\beta^2(\Omega^2 - K^2)}{\Omega^2}\right]^B e^{zB/H} F\left[B, 1 - A; 1 - A + B; \frac{\beta^2(K^2 - \Omega^2)}{\Omega^2} e^{z/H}\right] \right\} . \tag{32}$$

Thus, for the range of parameters (31), the dispersion relation is given by

$$\frac{\Gamma(B - A)}{[\Gamma(B)]^2} \left[\frac{\beta^2(\Omega^2 - K^2)}{\Omega^2}\right]^A F\left[A, 1 - B; 1 - B + A; \frac{\beta^2(K^2 - \Omega^2)}{\Omega^2}\right]$$
$$+ \frac{\Gamma(A - B)}{[\Gamma(A)]^2} \left[\frac{\beta^2(\Omega^2 - K^2)}{\Omega^2}\right]^B F\left[B, 1 - A; 1 - A + B; \frac{\beta^2(K^2 - \Omega^2)}{\Omega^2}\right] = 0 . \tag{33}$$

The dispersion relation (eq. [29] or [33]) has been evaluated for various values of the nondimensional parameter $\beta^2$. Examples are plotted in Figures 1 and 2 (also see Fig. 4). The curves in these figures represent well-defined eigenmodes of wave propagation in the atmosphere. These curves represent trapped waves propagating horizontally in the wave guide formed by the solid boundary below and the exponentially increasing Alfvén velocity above.

There are several ways of interpreting the effect of changing $\beta^2$ on the dispersion relation. First, different values of $\beta^2$ can be taken to represent the same magnetic field strength and the same density at $z = 0$, but different atmospheric temperatures. A second interpretation is that different values of $\beta^2$ represent the same magnetic field strength and the same temperature, but different densities. This is equivalent to placing the solid lower boundary at successively higher levels in the atmosphere corresponding to larger values of $\beta^2$. At each higher level the magnetic restoring force becomes more important due to the decreased density, while the compressible restoring force remains the same.

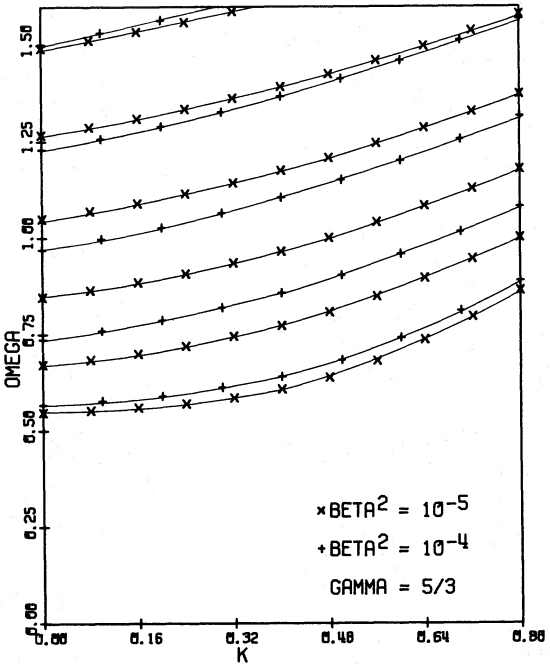


FIG. 1

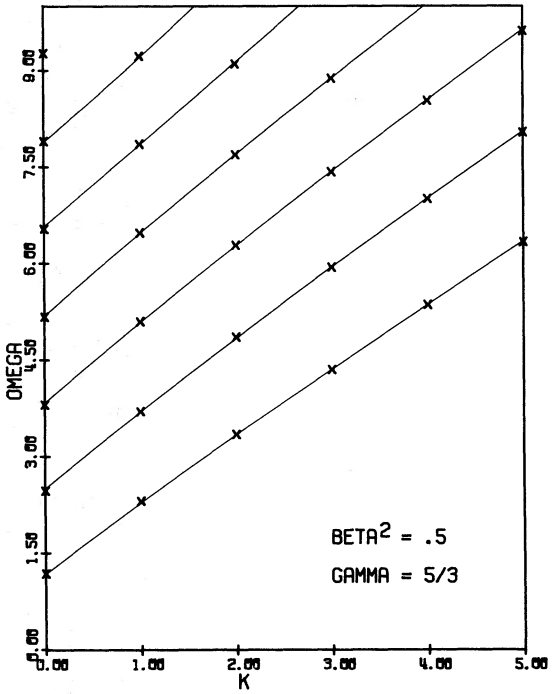


FIG. 2

FIG. 1.—Dispersion diagrams (nondimensional frequency versus nondimensional horizontal wavenumber) for an isothermal atmosphere with a uniform horizontal magnetic field and a solid lower boundary, with $\gamma = 5/3$, $\beta^2 = 10^{-5}$, and $\beta^2 = 10^{-4}$. The curves represent eigenmodes, and the crosses indicate the computed points. This figure should not be confused with a diagnostic diagram for an atmosphere with constant parameters (e.g., Yu 1965).

FIG. 2.—Same as Fig. 1, but with $\beta^2 = 0.5$.

The third interpretation is to consider changes in $\beta^2$ to be due to changes in the magnetic field strength, with fixed values of temperature and density. Since the sound speed and the density scale height then do not change, the scales for the frequency and horizontal wavenumber are the same in each case and the dispersion diagrams can be compared directly. From Figures 1 and 2 it can be seen that increasing the magnetic field strength (increasing $\beta^2$) increases the cutoff frequency. As $\beta^2$ increases, the slope of the dispersion curves, and hence the group velocity, also increases.

Lowering the value of $\gamma$ to represent crudely the effect of radiative transfer has little effect on the nondimensional dispersion diagrams. However, the frequency scaling depends on $\gamma$ as $\omega \sim (\gamma)^{1/2}\Omega$, while the wavenumber scaling is independent of $\gamma$. Therefore, for lower $\gamma$ (lower sound speed) the wave oscillates less rapidly and the phase and group velocities are correspondingly lower.

The vertical velocity of the disturbance (eq. [26] or [32]) can be calculated as a function of height for any point on a dispersion curve. Figure 3 compares the lowest mode of oscillation for the same horizontal wavenumber but different values of $\beta^2$ (i.e., different magnetic field strengths), and shows that for increasing magnetic field strength, the wave oscillates more rapidly and is trapped at lower levels in the atmosphere. We now discuss the eigenmodes given by the dispersion relation (29) or (33) in relation to an observed solar oscillation.

## V. APPLICATION TO FLARE-INDUCED CORONAL WAVES

On 1963 September 20, Moreton and Ramsey (Moreton 1965) observed a chromospheric disturbance, apparently caused by the flash phase of a flare, propagate at a nearly constant velocity of 750 km $s^{-1}$ for several hundred thousand kilometers across the solar disk. Many other flare-induced disturbances have been reported (Moreton 1960; Athay and Moreton 1961; Dodson and Hedeman 1968), and the propagation velocity is usually on the order of 1000 km $s^{-1}$. Dodson and Hedeman (1968) report that the width of the disturbance created by the proton flare of 1966 August 28 was greater than 100,000 km.

These disturbances could not have been propagating solely in the chromosphere, since in the chromosphere the sound speed is only of the order of 20 km $s^{-1}$ and the Alfvén velocity is only of the order of 50 km $s^{-1}$. Thus a purely chromospheric disturbance would have created a shock wave and been rapidly dissipated. In the corona, however, both the Alfvén velocity and the sound speed are an order of magnitude higher than in the chromosphere due to the increased temperature and decreased density. It has been proposed (Meyer 1968; Uchida 1968, 1970,

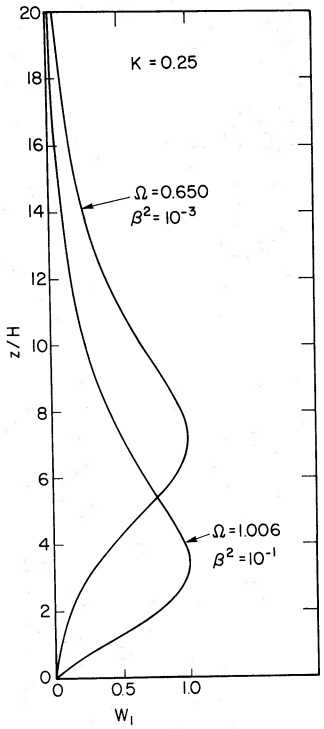


FIG. 3.—Direct comparison of the first mode of oscillation of the atmosphere for the same nondimensional horizontal wavenumber ($K = 0.25$) but for two values of $\beta^2$ ($\beta^2 = 10^{-3}$, $\beta^2 = 10^{-1}$).

1974; Uchida *et al.* 1973) that the disturbance is a magnetohydrodynamic wave propagating in the low corona and that the motion of this wave at the corona-chromosphere transition region is what is actually observed. There is, however, no general agreement as to the wavelength of the disturbance or even whether the observed disturbance is a single wave or a wave packet.

Meyer (1968) studied the propagation of the magnetoacoustic fast mode in an isothermal corona permeated by a uniform vertical magnetic field, with a rigid lower boundary representing the chromosphere-corona transition region. He found eigenmodes with nearly constant horizontal group velocity. Equating the group velocity to the observed propagation velocity, Meyer found that for a horizontal wavelength on the order of 100,000 km, the coronal magnetic field must be approximately 6 gauss, a reasonable average value.

Uchida, in a series of papers (Uchida 1968, 1970, 1974; Uchida *et al.* 1973), studied the propagation of short-wavelength ($\sim$5000 km) disturbances in various realistic coronal models. Using a ray-tracing technique, he obtained horizontal and vertical refractions in close agreement with the observed waves.

Although the magnetic field structure of the corona is quite complicated, the field changes fairly slowly and there are probably regions of nearly uniform field with almost any orientation. We study the case of a uniform horizontal field in connection with the coronal wave problem only as a means of understanding the mechanism of wave propagation for waves of arbitrary wavelength. Our model supplements Meyer's (1968) work by considering the case of a uniform horizontal magnetic field, and by including effects of gravity and stratification. As in Meyer's model, we use the rigid lower boundary to represent upward reflection from the chromosphere-corona transition layer.

We have evaluated our solution for a temperature of $1.6 \times 10^6$ K and $\beta^2 = 10$, which is fairly typical of the base of the corona. These values correspond to a sound speed of 180 km s$^{-1}$ and a density scale height of approximately 71,000 km. Figure 4 shows the dimensional dispersion relation for these parameters. We see that the dispersion curves are nearly straight, which means that these modes have very little dispersion and will propagate for great distances with little change in character. The first three modes have been calculated for a wavelength of 75,000 km in Figure 5. The first mode has nearly zero vertical velocity above two scale heights and is therefore trapped in the low corona.

The phase velocity and group velocity of the first mode have been plotted as a function of horizontal wavenumber in Figure 6. For any wavelength of 100,000 km or less, the group velocity is nearly constant at about 610 km s$^{-1}$. Since the energy of a disturbance propagates at the group velocity, it is not important which specific wavelength, or spectrum of wavelengths, receives energy from the flare. The energy at all wavelengths will propagate together as a wave packet near the lower coronal boundary.

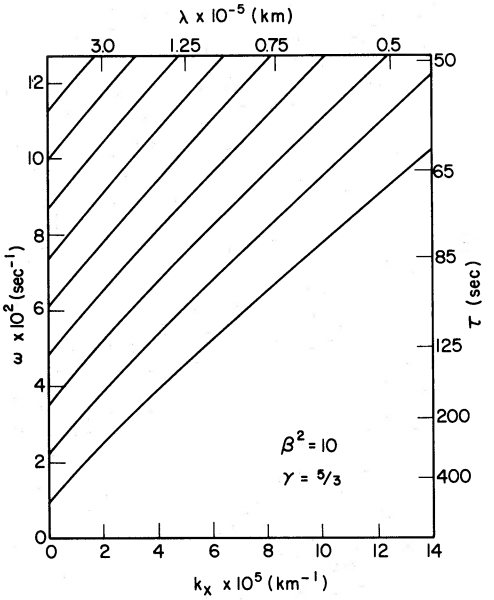


FIG. 4.—Dimensional dispersion diagram for $\beta^2 = 10$, $\gamma = 5/3$, and $T_0 = 1.6 \times 10^6$ K. The curves represent eigenmodes of the corona which are trapped by the increasing Alfvén velocity with height.

The present model is not proposed as a realistic model of the solar corona, although it may be fairly accurate over certain regions. No attempt has been made to include the effects of horizontal variations. The value of the model is that a mechanism for wave propagation can be studied for arbitrary wavelengths. These results close the gap between the short-wavelength ray-tracing theory and the long wavelength, vertical field case. We show that the question of wavelength is not particularly important since the group velocity of the trapped modes is essentially independent of wavelength. For the relatively large value of $\beta^2$ ($=10$), the wave modes are basically the magneto-acoustic fast modes (studied by Meyer and by Uchida) modified by gravity. For an inclined magnetic field, there must also be trapped modes of propagation involving a coupling of the present modes and the type of mode studied by Meyer for a vertical field. The present results, taken with those of Meyer and the work of Uchida, present a consistent picture of flare-induced coronal waves as guided magneto-atmospheric waves.

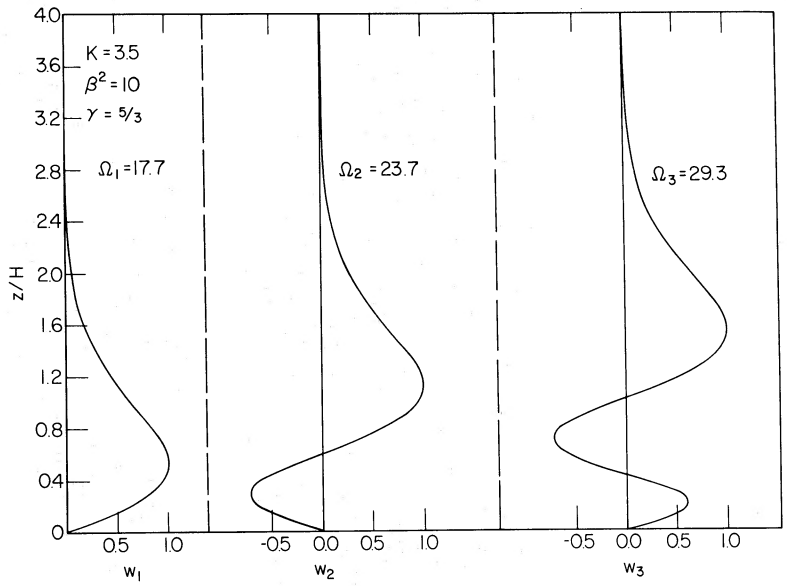


FIG. 5.—First three modes of oscillation of the model corona for $\beta^2 = 10$, $\gamma = 5/3$. The vertical velocities have been normalized to maximum value unity.

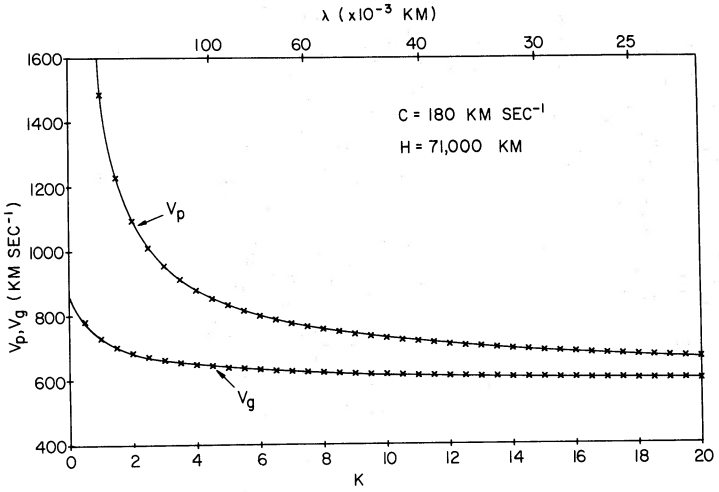


FIG. 6.—Phase velocity $v_p$ and group velocity $v_g$ of the first mode of coronal oscillation plotted as a function of horizontal wavenumber.

Much of this work was done while we were guests of the Max-Planck-Institut für Physik und Astrophysik in München, Germany. We are grateful to Professor Biermann for the hospitality of the Institut, and to Drs. H. U. Schmidt, Friedrich Meyer, John Stewart, and Tadashi Hirayama for helpful discussions. We also thank Professor Alfred Clark, Jr., at Rochester for helpful comments. One of us (A. H. N.) was supported by a National Science Foundation Predoctoral Traineeship. This work was supported by Air Force contract F 19628-75-C-0011 through Sacramento Peak Observatory, and by the Office of Naval Research.

## REFERENCES

Adam, J. A. 1975, Ph.D. thesis, University of London.
Athay, R. G., and Moreton, G. E. 1961, *Ap. J.*, **133**, 935.
Bel, N., and Mein, P. 1971, *Astr. and Ap.*, **11**, 234.
Chen, J. C., and Lykoudis, P. S. 1972, *Solar Phys.*, **25**, 380.
Dodson, H. W., and Hedeman, E. R. 1968, *Solar Phys.*, **4**, 229.
McLellan, A., and Winterberg, F. 1968, *Solar Phys.*, **4**, 401.
Meyer, F. 1968, in *IAU Symposium 35, Structure and Development of Solar Active Regions*, ed. K. Kiepenheuer (Dordrecht: Reidel), p. 485.
Michalitsanos, A. G. 1973, *Solar Phys.*, **30**, 47.
Moreton, G. E. 1960, *A.J.*, **65**, 494.
Moreton, G. E. 1965, in *IAU Symposium 22, Stellar and Solar Magnetic Fields*, ed. R. Lüst (Amsterdam: North-Holland), p. 371.
Nakagawa, Y., Priest, E. R., and Wellck, R. E. 1973, *Ap. J.*, **184**, 931.
Nye, A. H., and Thomas, J. H. 1974*a*, *Solar Phys.*, **38**, 399.
———. 1974*b*, *Bull. Am. Phys. Soc.*, **19**, 1148.
Thomas, J. H., and Nye, A. H. 1975, *Phys. Fluids*, **18**, 490.
Uchida, Y. 1968, *Solar Phys.*, **4**, 30.
———. 1970, *Pub. Astr. Soc. Japan*, **22**, 341.
———. 1974, *Solar Phys.*, **39**, 431.
Uchida, Y., Altsuchuler, M. D., and Newkirk, G., Jr. 1973, *Solar Phys.*, **28**, 495.
Yu, C. P. 1965, *Phys. Fluids*, **8**, 650.

ALAN H. NYE: Sacramento Peak Observatory, Sunspot, NM 88349

JOHN H. THOMAS: Department of Mechanical and Aerospace Sciences, University of Rochester, Rochester, NY 14627

THE ASTROPHYSICAL JOURNAL, 204:582–588, 1976 March 1


# SOLAR MAGNETO-ATMOSPHERIC WAVES. II. A MODEL FOR RUNNING PENUMBRAL WAVES

ALAN H. NYE AND JOHN H. THOMAS*
Department of Mechanical and Aerospace Sciences, University of Rochester
*Received 1975 June 20*

## ABSTRACT

A simple two-layer model of a sunspot penumbra is used to study the mode of running penumbral waves. Exact solutions of the linearized wave equation, not limited to the small-wavelength approximation, are employed in each layer. The lowest "plus" eigenmode of magneto-atmospheric waves in the model penumbra is in good agreement with observations of running penumbral waves. The results indicate that running penumbral waves should be observable in a photospheric spectral line.

*Subject headings:* hydromagnetics — Sun: atmospheric motions — Sun: magnetic fields — Sun: sunspots

## I. INTRODUCTION

In Paper I of this series (Nye and Thomas 1976) we presented an exact analytical solution for magneto-atmospheric waves in the case of an isothermal atmosphere with a uniform horizontal magnetic field. In the present paper we apply this solution to a simple two-layer model penumbra in order to study the mode of running penumbral waves.

Running penumbral waves (Zirin and Stein 1972; Giovanelli 1972, 1974; Moore and Tang 1975) are good examples of magneto-atmospheric waves. These waves propagate radially outward across sunspot penumbrae, with predominantly vertical motions in H$\alpha$. The observed range of frequency and propagation speed is fairly well established (see discussion in § IV).

Moore (1973) has concluded that the source of excitation of the penumbral waves is overstable convection in the low umbra. In an earlier paper (Nye and Thomas 1974 [NT]) we studied the mode of propagation of penumbral waves on the basis of a piecewise linear model of the vertical structure of a typical sunspot penumbra. We found the penumbral waves to be magneto-atmospheric waves (of the "plus" type) that are vertically trapped at photospheric levels. This trapping is primarily due to the increasing sound speed with depth into the convection zone and the increasing Alfvén velocity with height into the chromosphere.

Here we extend our earlier work by computing actual eigenmodes of propagation for a somewhat simpler model penumbra, which nevertheless retains the essential features. The properties of the lowest mode of propagation of the model penumbra turn out to be in good agreement with observations, and give some useful clues for further observation of running penumbral waves.

## II. THE TWO-LAYER PENUMBRAL MODEL

The entire penumbral model consists of a compressible, inviscid, perfectly conducting, stratified perfect gas subject to a constant acceleration of gravity $g$ ($=0.274$ km s$^{-2}$) in the negative $z$-direction. The upper layer is isothermal and is permeated by a uniform horizontal magnetic field, which yields an Alfvén velocity that increases exponentially with height due to the decreasing density. An exact solution of the linearized propagation equation for this case was given in Paper I.

This upper layer is a suitable model of the penumbral photosphere and chromosphere, where observed penumbral magnetic fields are very nearly horizontal (Nishi and Makita 1973) and decrease slowly with height (Bray and Loughhead 1964). The scale height for variation of the magnetic field is very large compared to the density scale height, so the assumption of the uniform horizontal magnetic field is reasonable. Our earlier calculations (NT) showed that running penumbral waves are trapped at photospheric levels, so that the increasing sound speed in the upper chromosphere has little effect on the trapping. Taking the upper layer to be isothermal is therefore also a reasonable assumption.

The vertical distributions of the sound speed and Alfvén velocity for the two-layer model penumbra are shown in Figure 1. Subscripts 1 and 2 denote quantities in the upper and lower layers, respectively, and the subscript 0

* Also C. E. Kenneth Mees Observatory.

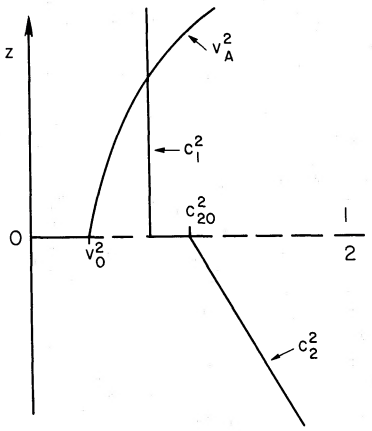


FIG. 1.—Distribution of $c^2$ and $v_A^2$ with height $z$ in the two-layer penumbral model. The upper layer (1) is isothermal with a uniform horizontal magnetic field. The lower layer (2) has an adiabatic temperature gradient and no magnetic field.

refers to quantities evaluated at $z = 0$. The sound speed, density scale height, and Alfvén velocity in the upper layer are given by

$$c_1^2 = \gamma_1 R T_1 = \text{const.}, \tag{1}$$

$$H_1 = \frac{c_1^2}{\gamma_1 g} = \text{const.}, \tag{2}$$

and

$$v_A^2(z) = v_0^2 \exp(z/H_1). \tag{3}$$

The lower layer of the penumbral model (layer 2, figure 1) is adiabatic with no magnetic field. The temperature decreases with height (increases with depth) at the adiabatic lapse rate, $(dT/dz)_s = -g/c_p$, and thus this layer is neutrally stable. The actual temperature distribution in the convection zone below a penumbra is probably very nearly adiabatic, except for a thin superadiabatic layer just beneath the photosphere that we neglect here. There is no magnetic field in this layer since we assume that the penumbral magnetic field lies over the convection zone. The sound speed squared and local density scale height each increases linearly with depth in the lower layer, their functional forms being

$$c_2^2(z) = c_{20}^2 - g(\gamma_2 - 1)z \tag{4}$$

and

$$H_2(z) = H_{20} - (\gamma_2 - 1)z. \tag{5}$$

The corresponding density distribution is

$$\rho_2(z) = \rho_{20}[1 - (\gamma_2 - 1)z/H_{20}]^{1/(\gamma_2 - 1)}. \tag{6}$$

At the interface between the two layers ($z = 0$), we require the undisturbed density to be continuous to avoid introducing interfacial gravity waves and wave reflections; therefore, $\rho_{10} = \rho_{20}$. In the unperturbed penumbra, there must be pressure equilibrium at the interface; that is, the gas pressure in the lower layer at $z = 0$ must equal the sum of the gas pressure and the magnetic pressure in the upper layer at $z = 0$. Therefore, the gas pressure is greater in layer 2 than in layer 1; and since the density is continuous across the interface, the temperature is greater in layer 2. This may be expressed in terms of the sound speeds and the Alfvén velocity at $z = 0$ as

$$c_{20}^2 = \frac{\gamma_2}{\gamma_1} c_1^2 + \frac{\gamma_2}{2} v_0^2. \tag{7}$$

We now turn to the problem of computing eigenmodes of magneto-atmospheric waves in this penumbral model.

## III. ANALYSIS

Consider first the behavior of small adiabatic perturbations in the lower layer (layer 2), an adiabatic atmosphere without magnetic field. Leibacher (1971) solved this problem in his study of oscillations of the quiet photosphere. Here we take a slightly different approach from his, using other transformations which yield a different form of the

propagation equation. For vanishing magnetic field ($\boldsymbol{B}_0 = \boldsymbol{B} = 0$), the vector equation for the perturbation velocity (eq. [7], Paper I) becomes

$$\frac{\partial^2 \boldsymbol{u}_2}{\partial t^2} = c_2{}^2 \nabla\phi + (\gamma_2 - 1)\phi \boldsymbol{g} + \nabla(\boldsymbol{u}_2 \cdot \boldsymbol{g}) , \tag{8}$$

where $\phi = \nabla \cdot \boldsymbol{u}_2$.

We assume that the perturbation velocity has the form $\boldsymbol{u}_2 = \hat{\boldsymbol{u}}_2(z) \exp [i(k_x x - \omega t)]$, with propagation in the $x$-direction ($k_y = 0$). This implies that $\hat{v}_2 = 0$ and $\hat{\boldsymbol{u}}_2 = \hat{\boldsymbol{u}}_2(z) = [\hat{u}_2(z), 0, \hat{w}_2(z)]$. All other perturbation quantities are represented in a similar manner, with a caret denoting the $z$-dependent amplitude in each case. From the two components of equation (8) and the definition of $\phi$, we obtain the following relation:

$$\hat{w}_2(z) = \frac{g[\gamma_2 - c_2{}^2 k_x{}^2/\omega^2]\hat{\phi} - c_2{}^2 d\hat{\phi}/dz}{\omega^2 - g^2 k_x{}^2/\omega^2} . \tag{9}$$

The pressure perturbation can also be written in terms of $\hat{\phi}$, using the continuity and energy relations (see Paper I):

$$\hat{p}_2 = -\frac{i\rho_2 c_2{}^2}{\omega}\left[\frac{(\omega^2 - g^2\gamma_2/c_2{}^2)\hat{\phi} + g d\hat{\phi}/dz}{\omega^2 - g^2 k_x{}^2/\omega^2}\right] . \tag{10}$$

Upon substitution of equation (9) into the $z$-component of equation (8), we obtain the following second-order differential equation for $\hat{\phi}$:

$$\frac{d^2\hat{\phi}}{dz^2} + \left(\frac{1}{c_2{}^2}\frac{dc_2{}^2}{dz} - \frac{g\gamma_2}{c_2{}^2}\right)\frac{d\hat{\phi}}{dz} + \left[\frac{\omega^2}{c_2{}^2} - k_x{}^2 + \frac{g^2 k_x{}^2}{\omega^2 c_2{}^2}(\gamma_2 - 1) + \frac{g k_x{}^2}{\omega^2 c_2{}^2}\frac{dc_2{}^2}{dz}\right]\hat{\phi} = 0 . \tag{11}$$

The nondimensional frequency, horizontal wavenumber, and depth, based on the values of sound speed and density scale height in layer 2 at $z = 0$, are defined by

$$\Omega_2 \equiv H_{20}\omega/c_{20} , \qquad K_2 \equiv H_{20} k_x , \qquad \text{and} \qquad \tilde{z} \equiv z/H_{20} . \tag{12}$$

By transforming the independent and dependent variables according to

$$Y = \frac{2K_2}{\gamma_2 - 1} - 2K_2\tilde{z} , \qquad \psi = e^{Y/2}\hat{\phi} , \tag{13}$$

equation (11) assumes the form

$$Y\frac{d^2\psi}{dY^2} + (b - Y)\frac{d\psi}{dY} - a\psi = 0 , \tag{14}$$

where

$$a = \frac{(2\gamma_2 - 1)}{2(\gamma_2 - 1)} - \frac{\Omega_2{}^2}{2K_2(\gamma_2 - 1)} , \qquad b = \frac{(2\gamma_2 - 1)}{(\gamma_2 - 1)} . \tag{15}$$

Equation (14) is the standard form of Kummer's equation (see Abramowitz and Stegun 1964). The solutions of this equation are given in terms of Kummer's functions,

$$M(a, b; Y) = \frac{\Gamma(b)}{\Gamma(a)}\sum_{n=0}^{\infty}\frac{\Gamma(a + n)}{\Gamma(b + n)}\frac{Y^n}{n!} . \tag{16}$$

The general solution of equation (14) is

$$\psi(Y) = D_3 M(a, b; Y) + D_4 U(a, b; Y) , \tag{17}$$

where $D_3$ and $D_4$ are arbitrary constants and $U(a, b; Y)$ can be written in terms of Kummer's functions. To insure finite total perturbation energy, we must require that the vertical velocity of the perturbation vanish as $z \to -\infty$ or as $Y \to +\infty$. This in turn requires that $D_3 = 0$. The solution for $\hat{\phi}$ as a function of $\tilde{z}$ in the lower layer is then

$$\hat{\phi}(\tilde{z}) = D_4 \frac{\pi}{\sin \pi b} \exp\left\{-\left[\frac{K_2}{(\gamma_2 - 1)} - K_2\tilde{z}\right]\right\}\left\{\frac{M[a, b; 2K_2/(\gamma_2 - 1) - 2K_2\tilde{z}]}{\Gamma(1 + a - b)\Gamma(b)}\right.$$
$$\left. - \left[\frac{2K_2}{(\gamma_2 - 1)} - 2K_2\tilde{z}\right]^{1-b}\frac{M[1 + a - b, 2 - b; 2K_2/(\gamma_2 - 1) - 2K_2\tilde{z}]}{\Gamma(a)\Gamma(2 - b)}\right\} . \tag{18}$$

The vertical velocity and pressure perturbation are given in terms of $\hat{\phi}$ by equations (9) and (10).

The form of the solution in the upper layer has been given in Paper I, and we shall not repeat the analysis here. The general form for the vertical velocity in the upper layer that gives finite total perturbation energy is given in terms of hypergeometric functions by either

$$\hat{w}_1(z) = D_1 \exp(-zK_1/H_1) F\left[A, B; C; \frac{\Omega_1^2}{\beta^2(K_1^2 - \Omega_1^2)} \exp(-z/H_1)\right] \tag{19}$$

for

$$\left|\frac{\Omega_1^2}{\beta^2(K_1^2 - \Omega_1^2)}\right| < \exp(z/H_1), \tag{20}$$

or else by

$$\begin{aligned}\hat{w}_1(z) = D_1 \exp(-zK_1/H_1)\Bigg\{&\frac{\Gamma(C)\Gamma(B-A)}{[\Gamma(B)]^2}\left[\frac{\beta^2(\Omega_1^2 - K_1^2)}{\Omega_1^2}\right]^A \exp(zA/H_1) \\ &\times F\left[A, 1-B; 1-B+A; \frac{\beta^2(K_1^2 - \Omega_1^2)}{\Omega_1^2}\exp(z/H_1)\right] \\ &+ \frac{\Gamma(C)\Gamma(A-B)}{[\Gamma(A)]^2}\left[\frac{\beta^2(\Omega_1^2 - K_1^2)}{\Omega_1^2}\right]^B \exp(zB/H_1) \\ &\times F\left[B, 1-A; 1-A+B; \frac{\beta^2(K_1^2 - \Omega_1^2)}{\Omega_1^2}\exp(z/H_1)\right]\Bigg\}\end{aligned} \tag{21}$$

for

$$\left|\frac{\Omega_1^2}{\beta^2(K_1^2 - \Omega_1^2)}\right| > \exp(z/H_1). \tag{22}$$

Here

$$A + B = C = 2K_1 + 1, \tag{23}$$

$$AB = \Omega_1^2 + K_1 + \left(\frac{\gamma_1 - 1}{\gamma_1^2}\right)\frac{K_1^2}{\Omega_1^2}, \tag{24}$$

$$\beta^2 = v_0^2/c_1^2, \tag{25}$$

and $\Omega_1$ and $K_1$ are nondimensional frequency and wavenumber defined as in (12), except sealed with $c_1$ and $H_1$.

The pressure perturbation in the upper layer consists of the sum of the gas pressure perturbation and the magnetic pressure perturbation. The gas pressure perturbation can be expressed in terms of the vertical velocity and its derivative as

$$\hat{p}_1 = -i\rho_1 c_1^2 \omega\left(\frac{d\hat{w}_1}{dz} - \frac{g}{c_1^2}\hat{w}_1\right)\Big/(\omega^2 - c_1^2 k_x^2). \tag{26}$$

The magnetic pressure perturbation $\hat{p}_m$ is found from the linearization of

$$p_m + \hat{p}_m = \frac{(\boldsymbol{B}_0 + \hat{\boldsymbol{B}})\cdot(\boldsymbol{B}_0 + \hat{\boldsymbol{B}})}{8\pi},$$

where $p_m$ is the unperturbed magnetic pressure. The components of the perturbed magnetic field are determined by the linearized induction equation (eq. [4] of Paper I). We find

$$\hat{p}_m = -i\frac{v_A^2\rho_1}{\omega}\frac{d\hat{w}_1}{dz} \tag{27}$$

The total perturbed pressure $\hat{p}_{T_1}$ in layer 1 is expressed in terms of the density and the Alfvén velocity as

$$\hat{p}_{T_1} = -\frac{i\rho_1}{\omega}\left\{[(c_1^2 + v_A^2)\omega^2 - c_1^2 v_A^2 k_x^2]\frac{d\hat{w}_1}{dz} - \omega^2 g\hat{w}_1\right\}\Big/(\omega^2 - c_1^2 k_x^2). \tag{28}$$

## IV. EIGENMODES AND RUNNING PENUMBRAL WAVES

We now have expressions for the vertical velocity and the pressure perturbation in each layer of the penumbral model, such that the total perturbation energy is finite. The remaining conditions are the matching of the vertical velocity and the perturbed pressure at the interface $z = 0$.

The scaling of frequency and wavenumber was done separately for each layer in order to simplify the propagation equation as much as possible in each case. In matching across the interface, we need the following relations between parameters in the two layers:

$$H_{20} = \gamma_2(1 + \tfrac{1}{2}\beta^2\gamma_1)H_1 , \tag{29}$$

$$\Omega_2^2 = \gamma_1\gamma_2(1 + \tfrac{1}{2}\beta^2\gamma_1)\Omega_1^2 , \tag{30}$$

$$K_2^2 = \gamma_2^2(1 + \tfrac{1}{2}\beta^2\gamma_1)^2K_1^2 , \tag{31}$$

and equation (7).

Continuity of the vertical velocity across $z = 0$ requires, after normalization, that

$$\hat{w}_1(0) = \hat{w}_2(0) = 1 . \tag{32}$$

This condition fixes the values of the coefficients $D_1$ in equation (19) or (21) and $D_4$ in equation (18). The remaining condition, the continuity of the perturbed pressure, requires that we equate (10) and (28). This then leads to the nondimensional condition

$$\left\{\frac{[(1 + \beta^2)\Omega_1^2 - \beta^2K_1^2](d\hat{w}_1/d\tilde{z}_1)|_0 - (\Omega_1^2/\gamma_1)\hat{w}_1(0)}{\Omega_1^2 - K_1^2}\right\} = \frac{1}{\gamma_1}\left[\frac{\Omega_2\gamma_2\tilde{\phi}(0) + (d\tilde{\phi}/dz_2)|_0}{\Omega_2^2 - K_2^2/\Omega_2^2}\right] , \tag{33}$$

where $\tilde{\phi} = \hat{\phi}H_{20}$. Equation (33) is only satisfied by particular values of frequency and wavenumber, and gives the dispersion relation for eigenmodes of oscillation in the penumbral model.

In order to evaluate the dispersion relation (33), the free parameters $\beta^2$, $\gamma_1$ and $\gamma_2$ must be specified, which then effectively determines the properties of the model. Although it is possible to evaluate (33) for different values of $\gamma$ in each layer (for example, a lower value of $\gamma_1$ could be taken to represent radiative transfer in the upper layer), we chose the usual value of 5/3 for both layers. The dispersion relation (33) was solved numerically by inserting values of $K_1$ and then computing and comparing the two sides of (33) for small increments in $\Omega_1$.

Figure 2 shows the first several eigenmodes of the two-layer penumbral model for $\beta^2 = 0.5$ and $\gamma_1 = \gamma_2 = 5/3$. The value of $\beta^2$ was chosen to represent a typical penumbra and is slightly less than the value of $\beta^2$ at $z = 0$ in our earlier penumbral model (*NT*). Here we have classified the eigenmodes as "plus" or "minus" modes, following the terminology used in the case of an atmosphere with constant spound speed, density scale height, and Alfvén velocity (see McLellan and Winterberg 1968 and NT). The plus modes all lie above the upper dashed line $\Omega = K$ in Figure 2, which corresponds to $\omega = c_1k_x$ (the Lamb mode). The minus mode (there is only one in this case) lies below the lower dashed line $\Omega = \beta K$ which corresponds to $\omega = v_0k_x$. There are no eigenmodes in the region between the dashed lines. This classification of plus or minus modes refers here to the character of the eigenmode

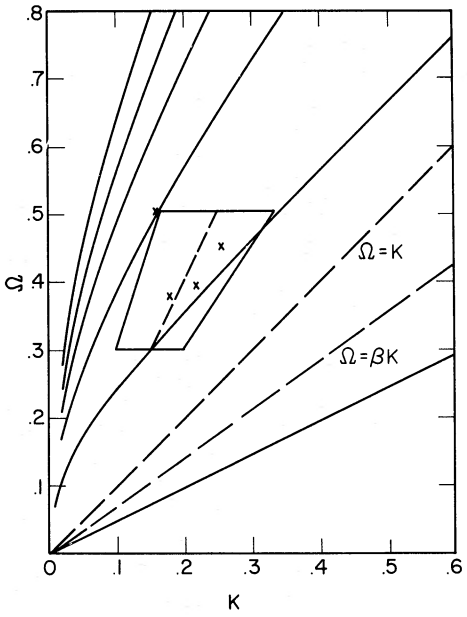


FIG. 2.—The first five plus eigenmodes and the only minus eigenmode of the two-layer penumbral model for $\beta^2 = 0.5$, $\gamma_1 = \gamma_2 = 5/3$. The quadrangle represents the range of observational data (see text). The crosses correspond to particular observations (Giovanelli 1974).

in the upper layer; in the lower layer, all of the modes have the character of acoustic waves (no magnetic field and no buoyancy).

Observational data on penumbral waves are included in Figure 2 for comparison. The most commonly reported observational quantities are the period and the horizontal phase velocity, although they are not always measured simultaneously. Giovanelli (1974) reports a typical phase velocity of running penumbral waves of 15 km $s^{-1}$ and typical periods in the range of 180–240 s. He did report phase velocities of up to 21 km $s^{-1}$, however, and gave specific periods and wavelengths for four sunspots (denoted by crosses in Fig. 2). The data of Beckers and Schultz (1972) appear to indicate a penumbral oscillation period of 255 s. Moore and Tang (1975) observed penumbral waves with period 270 $\pm$ 10 s in a single sunspot. Zirin and Stein (1972) state that the periods of penumbral waves in 20 sunspots were almost all between 240 and 300 s, and the measured horizontal phase velocity of 9.4 km $s^{-1}$ in one spot was more or less the same in other spots even when the period varied.

The quadrangle in Figure 2 represents the range of observations: periods from 180 to 300 s, and phase velocities from 9.4 to 21 km $s^{-1}$, with a dashed line at 15 km $s^{-1}$ to indicate the value that Giovanelli considers typical. The first plus mode of the penumbral model passes through this quadrangle. Although the particular eigenmode of oscillation of the penumbra is determined by the excitation, the details of which are uncertain, the present results indicate that it is the first plus eigenmode that is being excited. This agrees with our earlier conclusions (NT).

The value $\beta^2 = 0.5$ used in Figure 2 was chosen to represent a typical penumbra. In Figure 3 the effect of changes in $\beta^2$ on the first plus mode is shown for a range of $\beta^2$ of two orders of magnitude (0.05, 0.5, 5.0). This constitutes a reasonable set of limits on $\beta^2$ for penumbral conditions, and is obtained by looking at the normal variation of $B$ (factor of 4), $\rho$ (factor of 4), and $c^2$ (factor of 1.5) expected in different penumbrae. We see that for any reasonable value of $\beta^2$, the penumbral model has a first plus mode within the range of observations.

The vertical distributions of velocity and kinetic energy of the first plus mode (for $\beta^2 = 0.5$) are shown in Figure 4 for $K_1 = 0.1995$ and $\Omega_1 = 0.3628$, corresponding to a horizontal wavelength $\lambda = 3{,}000$ km and period $\tau = 250$ s for $c_1^2 = 43.5$ km$^2$ s$^{-2}$. Here the nondimensional height is scaled everywhere by the density scale height in the upper layer, $H_1$. The velocity distribution is fairly symmetric, with the maximum amplitude occurring slightly above $z = 0$ in the penumbral photosphere. The kinetic energy, on the other hand, is almost entirely trapped in the lower layer (convection zone)with maximum energy just below the interface. The velocity amplitude decays slowly with height with a value of more than 25 percent of the maximum amplitude at a distance of 8 scale heights above the level of that maximum.

There is a discrepancy between the height of maximum velocity predicted here ($z \approx 100$ km) and that predicted in our earlier paper (NT, $z \approx 1000$ km). Here the Alfvén velocity increases exponentially with height above the photosphere, whereas in NT it increased linearly. Thus, the downward refraction of waves is much stronger in the

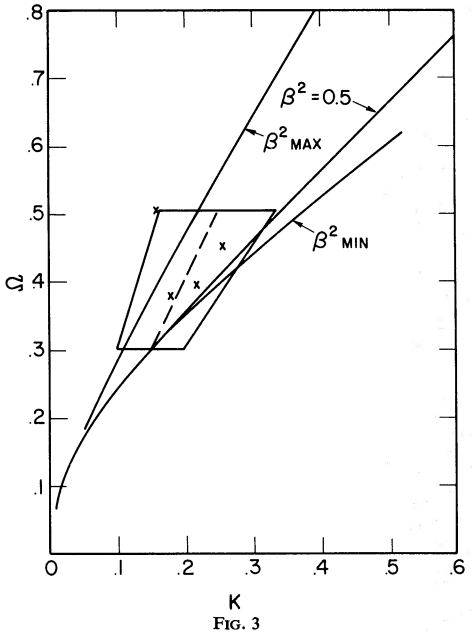


FIG. 3

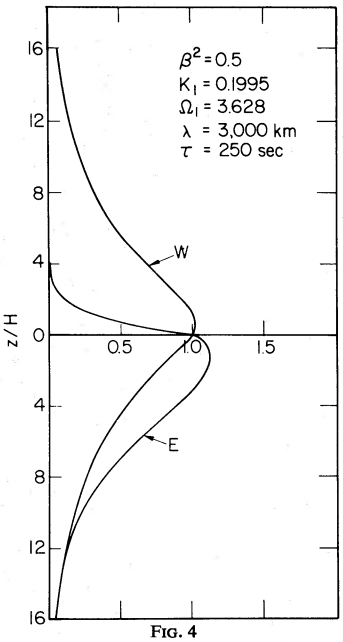


FIG. 4

FIG. 3.—The first plus eigenmode evaluated for extreme values of $\beta^2$ for sunspot penumbrae (see text): $\beta_{max}^2 = 5.0$, $\beta_{min}^2 = 0.05$. The quadrangle represents the range of observational data. The crosses correspond to particular observations (Giovanelli 1974).

FIG. 4.—The distribution of vertical velocity and kinetic energy of the first plus eigenmode with nondimensional height $z/H_1$. The velocity and energy are each normalized to value unity at the interface $z/H_1 = 0$.

present model. The actual situation is probably somewhere between these two cases. In either case, the wave energy lies mostly below the height of maximum vertical velocity, in the convection zone and low photosphere.

## V. CONCLUSIONS

The present results, taken together with our earlier work (NT), indicate that running penumbral waves should be identified with the lowest plus mode of trapped magneto-atmospheric waves in the penumbra. The vertical trapping is primarily due to the increasing Alfvén velocity up into the chromosphere and the increasing sound speed down into the convection zone. Most of the energy of the penumbral waves lies in the convection zone and low photosphere, at the same level as the expected source of excitation (umbral oscillatory convection). The maximum wave amplitude occurs somewhat higher.

The results also indicate that penumbral waves should be observable in a photospheric spectral line (see Fig. 4) as well as in H$\alpha$. There is some indication of this in the observation of Beckers and Schultz (1972). Their data show a 255 s period oscillation in the penumbra of one sunspot observed in a photospheric line. They present contours of vertical velocity as a function of horizontal position and time (their Fig. 1) in which one may note horizontal propagation outward across the penumbra at about the right phase speed. We plan further observations in a search for penumbral waves in the photosphere.

Much of this work was done while we were guests of the Max-Planck-Institut für Physik und Astrophysik in München, Germany. We are grateful to Professor Biermann for the hospitality of the Institut, and to Drs. H. U. Schmidt, Friedrich Meyer, John Stewart, and Tadashi Hirayama for helpful discussions. We also thank Professor Alfred Clark, Jr., at Rochester for helpful comments. One of us (A. H. N.) was supported by a National Science Foundation Predoctoral Traineeship. This work was supported by Air Force contract F 19628-75-C-0011 through Sacramento Peak Observatory, and by the Office of Naval Research.

## REFERENCES

Abramowitz, M., and Stegun, I. A. 1964, ed., *Handbook of Mathematical Functions* (Washington: National Bureau of Standards), p. 503.
Beckers, J. M., and Schultz, R. B. 1972, *Solar Phys.*, **27**, 61.
Bray, R. J., and Loughhead, R. E. 1964, *Sunspots* (London: Chapman & Hall), p. 212.
Giovanelli, R. G. 1972, *Solar Phys.*, **27**, 71.
———. 1974, in *IAU Symposium 56, Chromospheric Fine Structure*, ed. R. Grant Athay (Dordrecht: Reidel), p. 137.
Leibacher, J. W. 1971, Ph.D. thesis, Harvard University.
McLellan, A., and Winterberg, F. 1968, *Solar Phys.*, **4**, 401.
Moore, R. L. 1973, *Solar Phys.*, **30**, 403.
Moore, R. L., and Tang, F. 1975, *Solar Phys.*, **41**, 81.
Nishi, K., and Makita, M. 1973, *Pub. Astr. Soc. Japan*, **25**, 51.
Nye, A. H., and Thomas, J. H. 1974, *Solar Phys.*, **38**, 399 (NT).
———. 1976, *Ap. J.*, **204**, 573 (Paper I).
Zirin, H., and Stein, A. 1972, *Ap. J. (Letters)*, **173**, L85.

ALAN H. NYE: Sacramento Peak Observatory, Sunspot, NM 88349

JOHN H. THOMAS: Department of Mechanical and Aerospace Sciences, University of Rochester, Rochester, NY 14627